Available online at www.sciencedirect.com

ScienceDirect

ICARUS

Icarus 188 (2007) 522–534

www.elsevier.com/locate/icarus

Accretion of terrestrial planets from oligarchs in a turbulent disk

Masahiro Ogihara [a], Shigeru Ida [a,*], Alessandro Morbidelli [b]

[a] *Department of Earth and Planetary Sciences, Tokyo Institute of Technology, 2-12-1-I2-10 Ookayama, Meguro-ku, Tokyo 152-8551, Japan*
[b] *Observatoire de la Côte d'Azur, CNRS UMR 6202, BP 4229, 06304 Nice Cedex 4, France*

Received 30 July 2006; revised 13 December 2006

Available online 3 January 2007

Abstract

We have investigated the final accretion stage of terrestrial planets from Mars-mass protoplanets that formed through oligarchic growth in a disk comparable to the minimum mass solar nebula (MMSN), through N-body simulation including random torques exerted by disk turbulence due to Magneto-Rotational Instability. For the torques, we used the semi-analytical formula developed by Laughlin et al. [Laughlin, G., Steinacker, A., Adams, F.C., 2004. Astrophys. J. 608, 489–496]. The damping of orbital eccentricities (in all runs) and type-I migration (in some runs) due to the tidal interactions with disk gas is also included. Without any effect of disk gas, Earth-mass planets are formed in terrestrial planet regions in a disk comparable to MMSN but with too large orbital eccentricities to be consistent with the present eccentricities of Earth and Venus in our Solar System. With the eccentricity damping caused by the tidal interaction with a remnant gas disk, Earth-mass planets with eccentricities consistent with those of Earth and Venus are formed in a limited range of disk gas surface density ($\sim 10^{-4}$ times MMSN). However, in this case, on average, too many ($\gtrsim 6$) planets remain in terrestrial planet regions, because the damping leads to isolation between the planets. We have carried out a series of N-body simulations including the random torques with different disk surface density and strength of turbulence. We found that the orbital eccentricities pumped up by the turbulent torques and associated random walks in semimajor axes tend to delay isolation of planets, resulting in more coagulation of planets. The eccentricities are still damped after planets become isolated. As a result, the number of final planets decreases with increase in strength of the turbulence, while Earth-mass planets with small eccentricities are still formed. In the case of relatively strong turbulence, the number of final planets are 4–5 at 0.5–2 AU, which is more consistent with Solar System, for relatively wide range of disk gas surface density ($\sim 10^{-4}$–10^{-2} times MMSN).

Keywords: Planetary formation; Planet–disk interactions; Disks; Accretion; Terrestrial planets

1. Introduction

The final stage of terrestrial planet accretion would be coagulation among protoplanets (e.g., Lissauer, 1987). The protoplanets form through oligarchic growth (Kokubo and Ida, 1998, 2000), so that they are called 'oligarchs.' The protoplanets have almost circular orbits initially and are isolated from one another (Kokubo and Ida, 1998, 2000). Their mass is about Mars mass (Kokubo and Ida, 1998) in the case of the minimum mass solar nebula (MMSN) model (Hayashi, 1981). Long-term distant perturbations, however, would pump up eccentricities large enough for orbit crossing, on timescales that depend on mass of protoplanets and their orbital separation (Chambers et al., 1996). Because of relatively strong eccentricity damping due to tidal interaction with a gas disk (Artymowicz, 1993; Ward, 1993), the orbit crossing may not occur until disk gas surface density Σ_g decreases below $10^{-3}\Sigma_{g,\mathrm{MMSN}}$ (Iwasaki et al., 2002), where $\Sigma_{g,\mathrm{MMSN}}$ is the surface density of MMSN.

N-body simulations without any effect of disk gas (e.g., Chambers and Wetherill, 1998; Agnor and Canup, 1999) show that Earth-mass terrestrial planets are formed at ~ 1 AU in a disk with a solid surface density $\sim \Sigma_{d,\mathrm{MMSN}}$ as a result of the orbit crossing but with too large orbital eccentricities (~ 0.1) to be consistent with the present eccentricities of Earth and Venus in our Solar System. Kominami and Ida (2002, 2004) performed N-body simulations, taking into account the eccentricity damping caused by tidal interaction with a remnant gas disk and found that final eccentricities can be small enough to be consistent with those of Earth and Venus. The remnant disk with

* Corresponding author. Fax: +81 3 5734 3538.
E-mail address: ida@geo.titech.ac.jp (S. Ida).

0019-1035/$ – see front matter
doi:10.1016/j.icarus.2006.12.006

$\Sigma_g = 10^{-4}$–$10^{-3}\,\Sigma_{g,MMSN}$ allows orbit crossing, but it is still enough to damp eccentricities of Earth-mass planets to $\lesssim 0.01$ within disk depletion timescale $\sim 10^6$–10^7 years (Kominami and Ida, 2002; Agnor and Ward, 2002).

However, Kominami and Ida (2002, 2004) found that generally $\gtrsim 6$ planets remain in terrestrial planet region in strong damping cases. If the damping is weaker, number of planets decreases, while resultant eccentricities increase. Only in a limited range of the parameters, it sometimes occurs that Earth-mass planets with small enough eccentricities (Earth-like planets) are formed and total number of formed planets is $\lesssim 4$–5 in a disk similar to MMSN.

Chambers (2001), O'Brien et al. (2006), and Raymond et al. (2006) neglected the effects of a gas disk in their N-body simulations, but included dynamical friction from remnant planetesimals. Although the effect of the dynamical friction is essentially the same as the damping due to a gas disk, the number of formed planets is fewer while they have relatively small eccentricities. More detailed calculations are needed to clarify the role of dynamical friction from planetesimals.

Another possibility to reduce the number of formed planets while their eccentricities are kept small is a "shaking-up" process to inhibit isolation of planets due to the damping. If gas giants have already formed when the orbital crossing starts, eccentricity excitation by the secular perturbations from the gas giants can provide the shakes (e.g., Levison and Agnor, 2003). Kominami and Ida (2004) showed that perturbations from gas giants in the current orbits do not provide enough shakes in the presence of disk gas. However, O'Brien et al. (2006) reported that the secular perturbations from Jupiter and Saturn produce terrestrial planets more consistent with those in our Solar System in the case without the gas damping but with dynamical friction from planetesimals.

Nagasawa et al. (2005) considered a passage of a secular resonance during depletion of disk gas as a shaking-up mechanism and carried out N-body simulations. ν_5 resonance passes through ~ 1 AU when $\Sigma_g \sim 10^{-3}$–$10^{-2}\,\Sigma_{g,MMSN}$. Hence, after the eccentricity excitation and coagulation of protoplanets caused by the resonance passage, the disk gas is still able to damp the eccentricities (Eq. (14)). The damping induces inward orbital migration, so that bodies are captured by the resonances. The merged terrestrial planets, however, have to be released from the resonances at ~ 1 AU.

Here, we consider another shaking-up mechanism, random torques exerted by disk turbulence due to Magneto-Rotational Instability (MRI) (e.g., Balbus and Hawley, 1991). Laughlin et al. (2004) and Nelson and Papaloizou (2004) carried out fluid dynamical simulations of MRI and pointed out that the random torques may significantly influence orbital motions of planetesimals. Through analytical modeling, Johnson et al. (2006) also predicted significant orbital changes due to the random torques. Rice and Armitage (2003) studied accretion of a protoplanet taking into account the effect of random walks in semimajor axes induced by the random torques and found that the random walks expand effective feeding zone of the protoplanet and it may lead to rapid formation of a large core of a gas giant. However, since they did not integrate orbits directly, it is not clear if their incorporation of random torques is relevant. Actually, Nelson (2005) directly integrated orbits of protoplanets in a turbulent disk and found excitation of orbital eccentricities as well as random walks of semimajor axes. The eccentricity excitation was neglected in Rice and Armitage (2003). Because Nelson's (2005) orbital integration was done simultaneously with fluid dynamical simulation of MRI, the orbital integration was limited to 100–150 Keplerian times, which is too short to study accretion process of the protoplanets on $\gtrsim 10^6$ Keplerian times.

In order to perform N-body simulations long enough to calculate full stage of accretion of protoplanets, we adopt the semi-analytical formula for the random torque developed by Laughlin et al. (2004) based on their fluid dynamical simulations. We directly incorporate the random torques as forces acting on the protoplanets in the equations of motion. Hence, eccentricity excitation, which was neglected in Rice and Armitage (2003), is automatically included, as well as a random walk in semimajor axis. Because we do not perform fluid dynamical simulation, N-body simulations on timescales $\sim 10^7$ years are able to be done. The analytical formula may only roughly mimic the effects of MRI turbulence and the method by Nelson (2005) is more correct. However, our purpose is rather to explore the qualitative effects of the turbulence on orbital evolution and accretion of planets on long timescales and the dependence on the key parameters on the problem, so that a great quantitative accuracy is not important in the present contribution.

We also include the damping of eccentricities and inclinations directly in orbital integrations as forces acting on the protoplanets, essentially following Kominami and Ida (2002, 2004). However, we here adopt more exact forms of forces derived by Tanaka and Ward (2004) [also see Kominami et al. (2005) and Section 2.4]. Since in the turbulence, the effect of type-I migration might be greatly diminished (Nelson, 2005), we performed both simulations with type-I migration and those without it. When type-I migration is included, we adopt the formula for forces acting on the protoplanets derived by Tanaka and Ward (2004).

In Section 2, we describe the disk model, the formula of forces for the random torques, eccentricity damping and type-I migration. In Section 3.1, we present the results of one planet case in order to clearly see the effect of the random torques that we use, on the orbital evolution. The results of N-body simulations of accretion of protoplanets that start with 15 protoplanets of $0.2M_\oplus$ are shown in Section 3.2. We mainly consider the stage in which disk gas surface density has declined significantly so that the random torques are relatively weak. However, the weak random torques in the stage play important roles to produce terrestrial planets similar to those in our Solar System. Section 4 is the conclusion section.

2. Model and calculation methods

2.1. Disk model

Here, we consider a host star with $1M_\odot$. Following Ida and Lin (2004), we scale the gas surface density Σ_g of disks as

$$\Sigma_{\mathrm{g}} = 2400 f_{\mathrm{g}} \left(\frac{r}{1\ \mathrm{AU}}\right)^{-3/2} \mathrm{g\,cm^{-2}}, \tag{1}$$

where f_{g} is a scaling factor; $f_{\mathrm{g}} = 1$ corresponds to $\Sigma_{\mathrm{g}} = 1.4\Sigma_{\mathrm{g,MMSN}}$. Because current observations cannot strictly constrain the radial gradient of Σ_{g}, we here assume f_{g} is constant with r. Since we consider the stage where disk gas has been significantly depleted ($f_{\mathrm{g}} \leqslant 10^{-2}$), optical depth of the disk may be low. For simplicity, we use the temperature distribution in the limit of an optically thin disk (Hayashi, 1981),

$$T = 2.8 \times 10^2 \left(\frac{r}{1\ \mathrm{AU}}\right)^{-1/2} \mathrm{K}. \tag{2}$$

Corresponding sound velocity is

$$c_{\mathrm{s}} = 1.0 \times 10^5 \left(\frac{r}{1\ \mathrm{AU}}\right)^{-1/4} \mathrm{cm\,s^{-1}}. \tag{3}$$

2.2. Random torques due to MRI turbulence

Turbulence due to Magneto-Rotational Instability (Balbus and Hawley, 1991) is one of candidates to account for the observationally inferred disk viscosity, based on Hα line observation due to disk accretion onto stars (e.g., Hartmann et al., 1998). Gammie (1996) and Sano et al. (2000) pointed out the existence of "dead zone" around 1 AU where the degree of ionization is so small that MRI turbulence is suppressed. However, it is not clear that the dead zone exists in the last stage of terrestrial planet formation we are considering. If large fraction of dust grains have been transferred into planetesimals in the stage, ionization degree could be high enough that the dead zone disappears (Sano et al., 2000), although secondary dust production due to disruptive collisions between planetesimals may also be efficient in this stage (e.g., Inaba et al., 2003). On the other hand, Inutsuka and Sano (2005) proposed self-sustained ionization to suggest that dead zone vanishes, irrespective of degree of dust depletion. We here assume that disks are MRI-turbulent at $\sim$1 AU.

Laughlin et al. (2004) modeled the density fluctuations due to the MRI turbulence, based on their fluid dynamical simulation. Here we briefly summarize their results with slight modifications. The specific force due to density fluctuations exerted on a planet is given by

$$\boldsymbol{F}_{\mathrm{tub}} = -\Gamma \nabla \Phi, \tag{4}$$

where

$$\Gamma = \frac{64 \Sigma_{\mathrm{g}} r^2}{\pi^2 M_\odot}, \tag{5}$$

$$\Phi = \gamma r^2 \Omega^2 \sum_{i=1}^{50} \Lambda_{\mathrm{c},m}, \tag{6}$$

$$\Lambda_{\mathrm{c},m} = \xi e^{-(r-r_{\mathrm{c}})^2/\sigma^2} \cos(m\theta - \phi_{\mathrm{c}} - \Omega_{\mathrm{c}}\tilde{t}) \sin\left(\pi \frac{\tilde{t}}{\Delta t}\right). \tag{7}$$

In the above, m is the wavenumber, the dimensionless variable ξ has a Gaussian distribution with unit width, r and θ represent the location of the planet in cylindrical coordinates, $\Omega = \sqrt{GM_\odot/r^3}$ is Keplerian angular velocity at r, r_{c} and ϕ_{c} specify the center of the density fluctuation, and Ω_{c} is Ω at r_{c}. γ is the non-dimensional parameter to indicate the strength of the turbulence that we introduced instead of Laughlin et al.'s (2004) dimensional parameter A ($A = \gamma r^{5/2}\Omega^2$). The pattern speed Ω_{c} in the time-dependent factor allows the mode center to travel along with the Keplerian flow. With m specified, the mode extends for a distance $2\pi r_{\mathrm{c}}/m$ along the azimuthal direction. The radial extent is then specified by choosing $\sigma = \pi r_{\mathrm{c}}/4m$ so that the mode shapes have roughly a 4:1 aspect ratio. The total fluctuation is expressed by superposition of 50 modes at any given time. In Eq. (6), i in $\sum_{i=1}^{50}$ expresses individual modes. Each mode comes in and out of existence with the time dependence specified above. An individual mode begins at time t_0 and fades away when $\Delta t > \tilde{t} \equiv t - t_0$. The duration of the mode Δt is taken to be the sound crossing time of the mode along the angular direction, i.e., $\Delta t = 2\pi r_{\mathrm{c}}/m c_{\mathrm{s}}$. After the mode has gone, a new mode is generated. For the new mode, r_{c} is chosen randomly in the calculation area and ϕ is random in $0 \leqslant \phi < 2\pi$. The azimuthal wavenumber m is chosen to be distributed according to a log random distribution for wavenumbers in the range $2 \leqslant m \leqslant 64$.

We modify their formula in two points. The first one is introduction of the non-dimensional parameter γ for strength of turbulence. While Laughlin et al.'s (2004) simulation range was 1.5–3.5 AU, our simulations are done around 1 AU. Hence, it may be more useful to use the non-dimensional parameter than Laughlin et al.'s (2004) dimensional parameter A ($A = \gamma r^{5/2}\Omega^2$). Since Laughlin et al. (2004) used 3.4 AU and 1 year as units of length and time and the middle radius of their simulation was 2.5 AU, the values of A in their paper correspond to $\simeq 1.2\gamma(r/1\ \mathrm{AU})^{-1/2}$. Three-dimensional fluid dynamical simulations by Laughlin et al. (2004) suggest $\gamma \sim 10^{-3}$–10^{-2}, but the values of γ may include large uncertainty, so that we explore wide range of γ (also see discussion in Section 3.1). The second point is the range of wavenumber m. Although $2 \leqslant m \leqslant 64$ in the original formula given in Laughlin et al. (2004), inclusion of $m = 1$ modes could be more consistent with global fluid dynamical simulation (G. Laughlin, private communication; also see discussion in Section 3.1). On the other hand, modes with large m do not contribute to orbital changes, because of their short distances ($\sim\sigma = \pi r_{\mathrm{c}}/4m$) for effective forces and rapid time variations with timescale $2\pi r_{\mathrm{c}}/m c_{\mathrm{s}}$. Hence, in order to save calculation time, we cut off high m modes with $m \geqslant 6$, that is, $\Lambda_{\mathrm{c},m}$ is set to be zero when $m \geqslant 6$, in the summation of 50 modes in Eq. (6). The torque exerted on the planet with mass M is

$$\tau_{\mathrm{tub}} = r \times \frac{1}{r}\frac{\partial \Phi}{\partial \theta} \times \Gamma \times M \tag{8}$$

$$= -\gamma \Gamma M r^2 \Omega^2 \sum_{i=1}^{50} m \Lambda_{\mathrm{s},m}, \tag{9}$$

where

$$\Lambda_{\mathrm{s},m} = \xi e^{-(r-r_{\mathrm{c}})^2/\sigma^2} \sin(m\theta - \phi_{\mathrm{c}} - \Omega_{\mathrm{c}}\tilde{t}) \sin\left(\pi \frac{\tilde{t}}{\Delta t}\right). \tag{10}$$

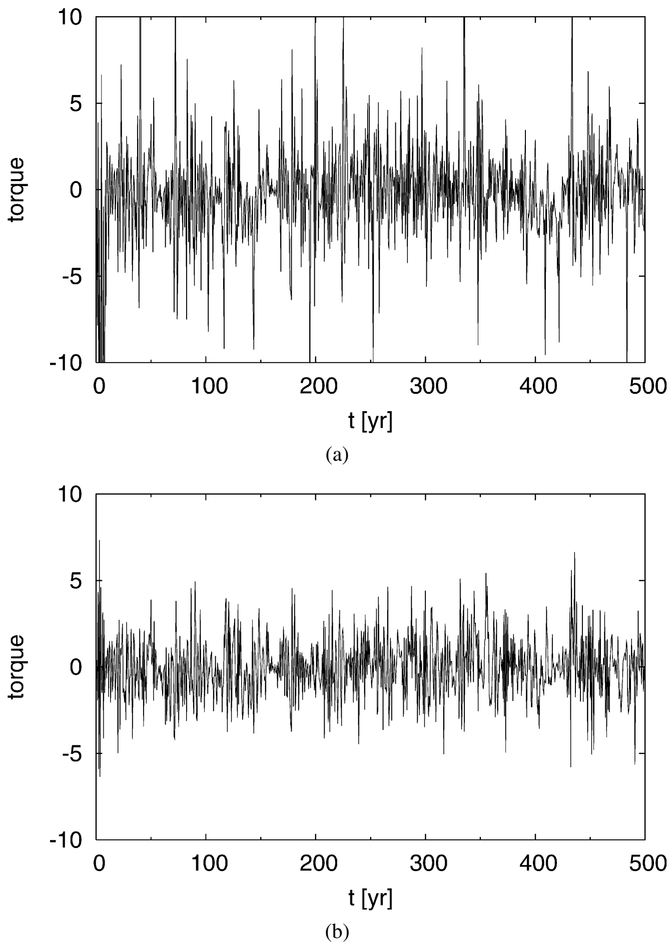

Fig. 1. An example of the random torques that we adopted. The (scaled) total torque $\sum_1^{50} m\Lambda_{\mathrm{s},m}$ is plotted (see Eq. (9)), as a function of time t: (a) the case of $2 \leqslant m \leqslant 64$ and (b) the case with the modes of $m \geqslant 6$ omitted (see Section 2.4).

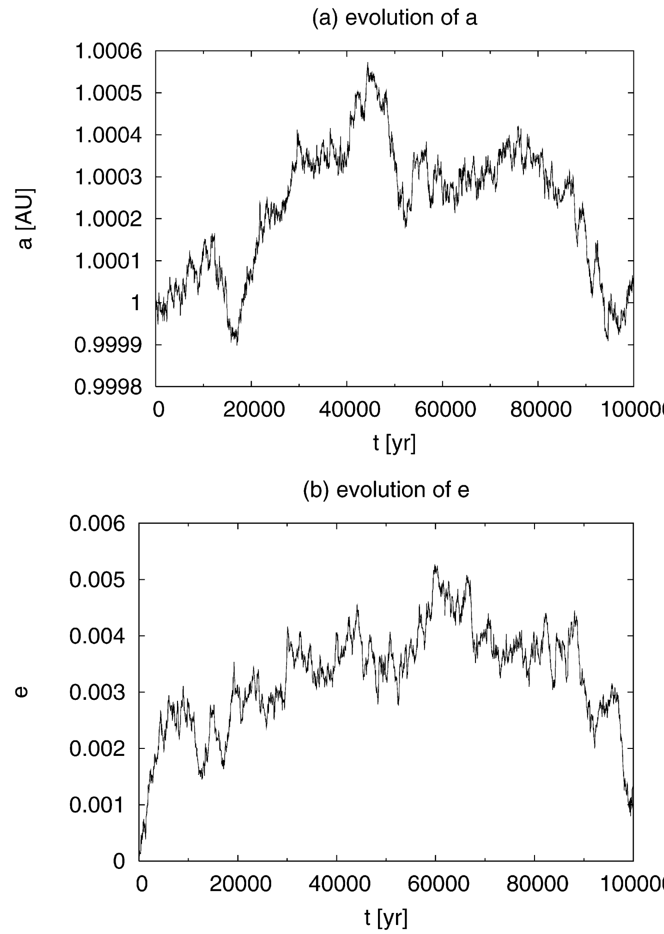

Fig. 2. Orbital evolution of a planet of $0.2M_\oplus$ suffering random torques due to turbulent fluctuations with $f_{\mathrm{g}} = 10^{-2}$ and $\gamma = 10^{-1}$. Type-I migration is not included. (a) Evolution of semimajor axis a and (b) that of orbital eccentricity e.

Fig. 1a shows the scaled random torques, $\sum_{i=1}^{50} m\Lambda_{\mathrm{s},m}$, with $2 \leqslant m \leqslant 64$. In Fig. 1b, $m \geqslant 6$ modes are cutted off. Low frequency patterns, which contribute to orbital evolution, are similar between these results. Actually, we found through orbital calculations like in Fig. 2 that $m \leqslant 5$ are enough to reproduce orbital evolution with fully counting all m modes. If $m = 1$ mode is included, the amplitude of the random torques does not change, but low frequency patterns change. We will present the results of N-body simulations with $2 \leqslant m \leqslant 5$ in Section 3.2, but we also carried out calculations with $1 \leqslant m \leqslant 5$ and will discuss the effects of $m = 1$ modes.

2.3. Secular torques due to disk–planet interactions

As shown below, the random torques given by Eq. (9) induce random walks of semimajor axes of planets and pump up their orbital eccentricities. Tidal interactions with a laminar disk monotonically decreases the semimajor axes and damp the eccentricities (and the inclinations). The secular inward migration is known as "type-I migration" (e.g., Ward, 1986, 1997; Tanaka and Ward, 2002). Since mean flow in turbulent disks coincides with flow in laminar disks, interactions with the mean flow may induce the secular orbital migration and eccentricity damping even in turbulent disks. In turbulent disks, however, Nelson (2005) reported that type-I migration might be greatly diminished while the eccentricity damping still works. Nonlinear effects associated with the random fluctuations (e.g., the temporary activation of corotation torques or temporary disruption of the pressure buffer) could be responsible for the slowing down. Alternatively, relatively high eccentricities excited by the random torques, which is $\gtrsim h/r \sim 0.05$ obtained by Nelson (2005), where h is disk scale height, could affect the type-I migration (e.g., Papaloizou and Larwood, 2000). In our N-body simulations, eccentricities are also pumped up to $\gtrsim 0.05$ by perturbations among protoplanets except for the last phases well after orbital crossing. Hence, we performed two series of simulations: one is without type-I migration and the other is with it.

We summarize the secular changes in laminar disks below. Both torques from inner and outer disks damp orbital eccentricities and inclinations, since the gravitational interactions with disk gas causes similar effect of dynamical friction. The damping timescales are (Tanaka and Ward, 2004)

$$t_{\mathrm{damp},e} = -\frac{e}{\dot{e}} = \frac{t_{\mathrm{damp}}}{0.78}, \tag{11}$$

$$t_{\mathrm{damp},i} = -\frac{i}{\dot{i}} = \frac{t_{\mathrm{damp}}}{0.54}, \tag{12}$$

$$t_{\rm damp} = \left(\frac{M}{M_\odot}\right)^{-1}\left(\frac{\Sigma_{\rm g}a^2}{M_\odot}\right)^{-1}\left(\frac{c_{\rm s}}{v_{\rm K}}\right)^4 \Omega^{-1} \tag{13}$$

$$= 240 f_{\rm g}^{-1}\left(\frac{M}{M_\oplus}\right)^{-1}\left(\frac{a}{1\ {\rm AU}}\right)^2 \text{ years}, \tag{14}$$

where a is the semimajor axis of the planet and $v_{\rm K}$ is the Keplerian velocity at a.

On the other hand, the torque from an inner disk increases semimajor axis, while that from an outer disk decreases it. Since the outer torque is generally greater than the inner one (Ward, 1986; Tanaka and Ward, 2002), the torque imbalance induces inward migration (type-I migration). For the radial gradient of $\Sigma_{\rm g} \propto a^{-1.5}$, the torque imbalance, which is negative definite, is given by (Tanaka and Ward, 2002)

$$\tau_{\rm mig} = -2.17\left(\frac{M}{M_\odot}\right)^2\left(\frac{v_{\rm K}}{c_{\rm s}}\right)^2 \Sigma_{\rm g} a^4 \Omega^2. \tag{15}$$

Migration timescale due to this torque is

$$t_{\rm mig} = -\frac{a}{\dot{a}} = \frac{(1/2)M\Omega a^2}{\tau_{\rm mig}} \tag{16}$$

$$= 0.23\left(\frac{M}{M_\odot}\right)^{-1}\left(\frac{\Sigma_{\rm g}a^2}{M_\odot}\right)^{-1}\left(\frac{c_{\rm s}}{v_{\rm K}}\right)^2 \Omega^{-1} \tag{17}$$

$$= 5.0\times 10^4\left(\frac{M}{M_\oplus}\right)^{-1}\left(\frac{a}{1\ {\rm AU}}\right)^{3/2} f_{\rm g}^{-1} \text{ years}. \tag{18}$$

2.4. Orbital integration

We integrate orbits of 15 protoplanets with $0.2M_\oplus$ that initially have orbits of small e and i ($\sim$0.01) with separation $6r_{\rm H}$, following initial conditions in Kominami and Ida (2002), where Hill radius $r_{\rm H}$ is defined by

$$r_{\rm H} = \left(\frac{M}{3M_\odot}\right)^{1/3} a \simeq 0.007\left(\frac{M}{0.2M_\oplus}\right)^{1/3} a. \tag{19}$$

Initial angular distributions are set to be random. Calculation starts from the phase when the orbital crossing starts. The result of Kokubo and Ida (2000) shows that the eccentricities of protoplanets produced through oligarchic growth are about $\sim 10^{-3}$, so that the protoplanets are well isolated. However, the protoplanets will eventually start orbital crossing by long-term mutual distant perturbations on a timescale depending on their orbital separation, mass (Chambers et al., 1996), initial eccentricities (Yoshinaga et al., 1999), and how much gas is around the protoplanets (Iwasaki et al., 2002). Since we are concerned with orbital crossing stage, we start the calculation with relatively high eccentricities $e = 10^{-2}$, supposing the eccentricities have already increased and orbital crossing is ready to start. The initial inclinations are also set to be $i = 10^{-2}$.

The basic equations of motion of particle k at r_k in heliocentric coordinates are

$$\frac{{\rm d}^2\boldsymbol{r}_k}{{\rm d}t^2} = -GM_\odot\frac{\boldsymbol{r}_k}{|\boldsymbol{r}_k|^3} - \sum_{j\neq k} GM_j\frac{\boldsymbol{r}_k-\boldsymbol{r}_j}{|\boldsymbol{r}_k-\boldsymbol{r}_j|^3} - \sum_j GM_j\frac{\boldsymbol{r}_j}{|\boldsymbol{r}_j|^3} + \boldsymbol{F}_{\rm damp} + \boldsymbol{F}_{\rm tub} + \boldsymbol{F}_{\rm mig}, \tag{20}$$

where $k, j = 1, 2, \ldots, 15$, the first term is gravitational force of the central star, the second term is mutual gravity between the bodies, and the third term is the indirect term. $\boldsymbol{F}_{\rm damp}$ and $\boldsymbol{F}_{\rm mig}$ are specific forces for the damping of eccentricities and inclinations and type-I migration, and $\boldsymbol{F}_{\rm tub}$ is specific force due to the turbulence (Eq. (4)). Their detailed expressions are described below. Note that in our simulations, mass of bodies is larger than $0.2M_\oplus$, so that aerodynamical drag forces are neglected compared with $\boldsymbol{F}_{\rm damp}$ and $\boldsymbol{F}_{\rm mig}$ (e.g., Ward, 1993).

We integrate orbits with the fourth-order Hermite scheme. When protoplanets collide, perfect accretion is assumed. After the collision, a new body is created, conserving total mass and momentum of the two colliding protoplanets. The physical radius of a protoplanet is determined by its mass and internal density as

$$r_{\rm P} = \left(\frac{3}{4\pi}\frac{M}{\rho_{\rm P}}\right)^{1/3}. \tag{21}$$

The internal density $\rho_{\rm P}$ is set to be $3\ {\rm g\,cm^{-3}}$.

Tanaka and Ward (2004) derived, through three-dimensional linear analysis,

$$F_{{\rm damp},r} = \left(\frac{M}{M_\odot}\right)\left(\frac{v_{\rm K}}{c_{\rm s}}\right)^4\left(\frac{\Sigma_{\rm g}r^2}{M_\odot}\right) \times \Omega\left(2A_r^{\rm c}[v_\theta - r\Omega] + A_r^{\rm s}v_r\right), \tag{22}$$

$$F_{{\rm damp},\theta} = \left(\frac{M}{M_\odot}\right)\left(\frac{v_{\rm K}}{c_{\rm s}}\right)^4\left(\frac{\Sigma_{\rm g}r^2}{M_\odot}\right) \times \Omega\left(2A_\theta^{\rm c}[v_\theta - r\Omega] + A_\theta^{\rm s}v_r\right), \tag{23}$$

$$F_{{\rm damp},z} = \left(\frac{M}{M_\odot}\right)\left(\frac{v_{\rm K}}{c_{\rm s}}\right)^4\left(\frac{\Sigma_{\rm g}r^2}{M_\odot}\right)\Omega\left(A_z^{\rm c}v_z + A_z^{\rm s}z\Omega\right), \tag{24}$$

$$F_{{\rm mig},r} = 0, \tag{25}$$

$$F_{{\rm mig},\theta} = -2.17\left(\frac{M}{M_\odot}\right)\left(\frac{v_{\rm K}}{c_{\rm s}}\right)^2\left(\frac{\Sigma_{\rm g}r^2}{M_\odot}\right)\Omega v_{\rm K}, \tag{26}$$

$$F_{{\rm mig},z} = 0, \tag{27}$$

where

$$A_r^{\rm c} = 0.057, \qquad A_r^{\rm s} = 0.176,$$
$$A_\theta^{\rm c} = -0.868, \qquad A_\theta^{\rm s} = 0.325,$$
$$A_z^{\rm c} = -1.088, \qquad A_z^{\rm s} = -0.871.$$

Note that there is a typos in $F_{{\rm damp},z}$ in Tanaka and Ward (2004). The factor $(2A_z^{\rm c}v_z + A_z^{\rm s}z\Omega)$ should be $(A_z^{\rm c}v_z + A_z^{\rm s}z\Omega)$ as in Eq. (24). Note also that the other factors in the expressions in Kominami et al. (2005) have minor typos; the above expressions are correct ones. Eccentricities are damped by $F_{{\rm damp},r}$ and $F_{{\rm damp},\theta}$, while inclinations are damped by $F_{{\rm damp},z}$. Semimajor axes are decreased by $F_{{\rm mig},\theta}$ $(= \tau_{\rm mig}/Mr)$, where a and r are identified because of small e and i. The evolution of e, i, and a by orbital integration of one body with the above forces completely agrees with the analytically derived evolution with Eqs. (14) and (18).

The force due to turbulence, $\boldsymbol{F}_{\rm tub} = -\Gamma \nabla \Phi$ (Eq. (4)), is given by

$$F_{{\rm tub},r} = \gamma \Gamma r \Omega^2 \sum_{i=1}^{50} \left(1 + \frac{2r(r - r_{\rm c})}{\sigma^2}\right) \Lambda_{{\rm c},m}, \tag{28}$$

$$F_{{\rm tub},\theta} = \gamma \Gamma r \Omega^2 \sum_{i=1}^{50} m \Lambda_{{\rm s},m}, \tag{29}$$

$$F_{{\rm tub},z} = 0, \tag{30}$$

where $\Lambda_{{\rm c},m}$ and $\Lambda_{{\rm s},m}$ are defined by Eqs. (7) and (10).

As seen above, $\boldsymbol{F}_{\rm damp}$ and $\boldsymbol{F}_{\rm mig}$ are parameterized by the disk surface scaling factor $f_{\rm g}$ for given M and r of planets, and $\boldsymbol{F}_{\rm tub}$ by $f_{\rm g}$ and γ ($\Gamma \propto f_{\rm g}$). Therefore, $f_{\rm g}$ and γ are parameters for our calculations. As discussed in Section 1, we will consider the stages in which disk gas has been significantly depleted, so that the cases of $f_{\rm g} = 10^{-4}$ and 10^{-2} are mainly studied. Although the most likely value of γ might be $\sim 10^{-3}$–10^{-2}, it would include large uncertainty (also see discussion in Section 3.1), so that the cases of $\gamma = 10^{-3}$, 10^{-1}, and 1 are studied. For comparison, non-turbulent ($\gamma = 0$) cases are also calculated.

3. Results

3.1. One planet case

To see the effects of the turbulent forces given by Eqs. (28) and (29) on orbital changes and how they depend on $f_{\rm g}$ and γ, we first carry out simulations with one planet embedded in a turbulent disk. Fig. 2 shows evolution of semimajor axis a and orbital eccentricity e of a planet of $0.2M_\oplus$ obtained by orbital integration with $\boldsymbol{F}_{\rm tub}$ in the case of $\gamma = 10^{-1}$ and $f_{\rm g} = 10^{-2}$. The initial conditions are $a = 1$ AU and $e = 0$. $\boldsymbol{F}_{\rm damp}$ and $\boldsymbol{F}_{\rm mig}$ are not included. As expected, a random walk of a and excitation of e are observed.

In order to quantify the random walks, we performed 100 similar runs with different random numbers for the random torques, but still using $\gamma = 10^{-1}$ and $f_{\rm g} = 10^{-2}$. At each time, the distributions of deviation in semimajor axis Δa from the initial position (1 AU) and orbital eccentricity e for the 100 runs are fitted as Gaussian distributions to obtain the standard deviations as functions of time. Hereafter, the standard deviations are also denoted by Δa and e. Fig. 3 shows the evolution of Δa and e obtained by the numerical calculations. The evolution curves are fitted as

$$\Delta a \sim 1.8 \times 10^{-6} \left(\frac{t}{1\ \text{year}}\right)^{1/2} \text{AU}, \tag{31}$$

$$e \sim 2.7 \times 10^{-5} \left(\frac{t}{1\ \text{year}}\right)^{1/2} \tag{32}$$

near 1 AU. The dependence of $t^{1/2}$ would reflect diffusion characteristics. (If $\boldsymbol{F}_{\rm damp}$ is included, e approaches an equilibrium value.) We have carried out the same procedures for $\gamma = 10^{-2}$, 10^{-1}, and $f_{\rm g} = 10^{-2}$, 10^{-1} to derive the dependence of γ

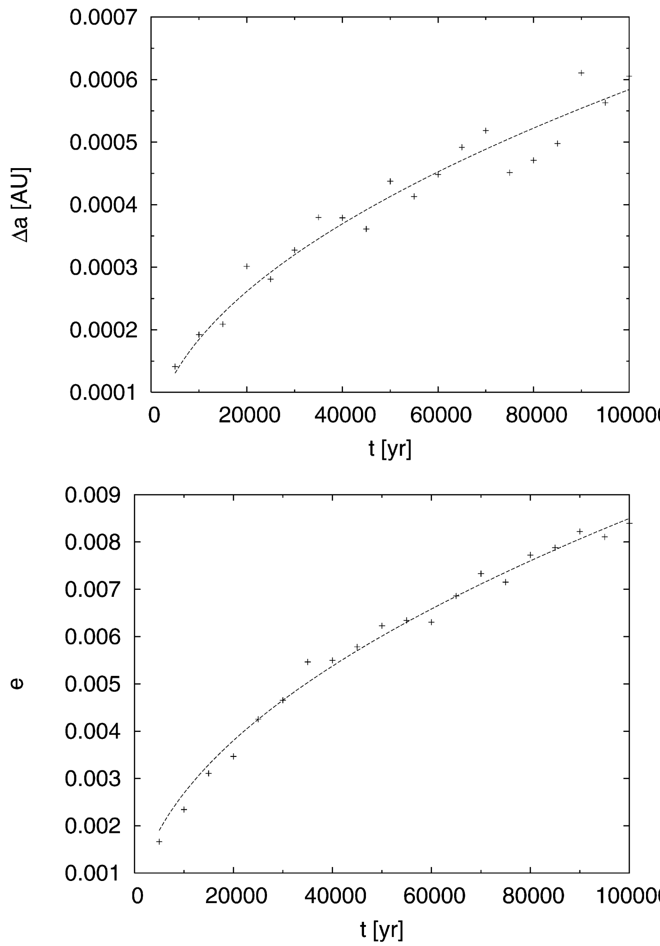

Fig. 3. Time evolution of dispersion of Δa and e. Crosses are the standard deviations of Gaussian distributions derived from 100 numerical integrations with different random numbers for random torques but with $f_{\rm g} = 10^{-2}$ and $\gamma = 10^{-1}$. The solid curves are fitted functions given by Eqs. (31) and (32).

and $f_{\rm g}$ as

$$\Delta a \sim 2 \times 10^{-3} f_{\rm g} \gamma \left(\frac{t}{1\ \text{year}}\right)^{1/2} \text{AU}, \tag{33}$$

$$e \sim 3 \times 10^{-2} f_{\rm g} \gamma \left(\frac{t}{1\ \text{year}}\right)^{1/2}. \tag{34}$$

Note that the random walks are independent of planet mass M. In the above calculations, we used $m = 2$–5 modes. With $m = 2$–64, we obtained very similar results.

Equations (33) and (34) give Δa and e that are 10–100 times smaller than those obtained by Laughlin et al. (2004) and Nelson (2005). We found that the analytically modeled random torques almost cancel out in time and the net change is only ~ 0.001 of total change for $m = 2$–5. Since both Laughlin et al. (2004) and Nelson (2005) used global fluid codes to follow orbits of protoplanets, $m = 1$ modes might be included. Since $m = 1$ modes have the longest duration and distance for effective force, it would induce asymmetry between positive and negative torques to produce larger Δa and e. We have carried out similar calculations, including $m = 1$ modes and found that Δa and e are 10 times larger than Eqs. (33) and (34). The inclusion of $m = 1$ modes may mostly resolve the difference

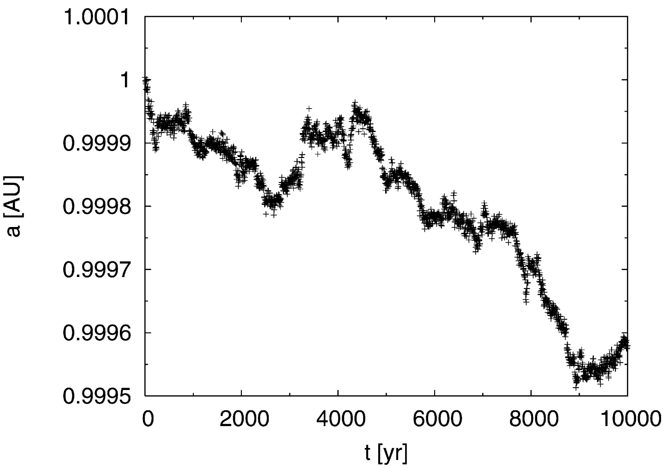

Fig. 4. Orbital evolution with both effects of type-I migration and turbulent fluctuations with $f_g = 10^{-2}$ and $\gamma = 10^{-1}$.

from the results by Laughlin et al. (2004) and Nelson (2005), but the approximated semi-analytical torque formula could be still too symmetric, compared with the global fluid dynamical simulations. Hence, the results of $\gamma = 10^{-1}$ and 1 (with $m = 2$–5 modes), which are larger than the numerically inferred value $\gamma \sim 10^{-3}$–10^{-2}, are also pertinent for the evolution of planets in realistic turbulent disks. In the N-body simulations shown in Section 3.2, perturbations from other protoplanets also induce some asymmetry and Δa and e may be much larger than Eqs. (33) and (34) during the period in which protoplanets undergo relatively close encounters.

If type-I migration works on the timescale given by Eq. (18), the migration length near 1 AU is

$$\Delta a \sim 2 \times 10^{-5} f_g \left(\frac{M}{M_\oplus}\right)\left(\frac{t}{1\ \text{year}}\right)\ \text{AU}. \tag{35}$$

From Eqs. (33) and (35), it is expected that if

$$t \gtrsim 3 \times 10^5 \gamma^2 \left(\frac{M}{0.2 M_\oplus}\right)^{-2}\ \text{years}, \tag{36}$$

type-I migration will dominate over the random walk. Fig. 4 shows the evolution of the semimajor axis with both effects of type-I migration and turbulent fluctuations of $\gamma = 0.1$. The planet starts secular inward migration after $t \sim 3 \times 10^3$ years, consistent with the above estimate. Note, however, that in the turbulent disks, it is not clear that type-I migration speed is still the same as that predicted by the linear calculation (Nelson, 2005).

3.2. Accretion of protoplanets in a turbulent disk

Because we will compare the results with Kominami and Ida (2002) and because type-I migration might be greatly diminished in turbulent disks, in many runs we calculate accretion and the orbital evolution of protoplanets in a turbulent disk without the effect of type-I migration. We carry out simulations with various f_g and γ. We denote a run with $f_g = 10^{-\alpha}$, $\gamma = 10^{-\beta}$ as RUN$\alpha_{\beta k}$, where k ($k = a, b, c$) represent different initial angular distribution of the protoplanets. In some runs, the effect of type-I migration is included, which we denote as RUN$\alpha_{\beta a \mathrm{I}}$. Table 1 shows simulation parameters for individual runs with $\gamma \leqslant 1$ and $m = 2$–5 (28 runs). Two runs were carried out with $\gamma = 10$ ($m = 2$–5). We also carried out 18 runs with inclusion of $m = 1$ modes and found that slightly smaller γ produce similar results to the cases without $m = 1$ modes. To avoid confusion, we will only present the detailed results with $m = 2$–5.

3.2.1. Case with $f_g = 10^{-2}$

First we show the results with $f_g = 10^{-2}$. The orbital evolution of RUN$2_{\infty a}$, RUN2_{3a}, RUN2_{1a}, and RUN2_{0a} is shown in Figs. 5a, 5b, 5c, and 5d, respectively. The thick solid lines represent semimajor axes a. The thin dashed lines represent pericenters $a(1-e)$ and apocenters $a(1+e)$. Thicker solid lines represent more massive planets. With $f_g = 10^{-2}$, the damping timescale $\tau_{\mathrm{damp}} \simeq 1.2 \times 10^5$ years for $M = 0.2 M_\oplus$.

Since RUN$2_{\infty a}$ does not include the random torques ($\gamma = 0$), the evolution in Fig. 5a is very similar to that shown by Kominami and Ida (2002). In this case, a planet of $0.6 M_\oplus$ with small eccentricity ($\sim$0.0001) is formed. However, global orbital crossing lasts for only $\sim 5 \times 10^5$ years because of the rather strong eccentricity damping. Consequently, the number of surviving planets is 8, which is much greater than that in the present Solar System. The runs with very weak turbulence of $\gamma = 10^{-3}$ in Fig. 5b show a similar result to the non-turbulent case. For $\gamma = 0$ and 10^{-3}, the number of surviving planets is always 8 or 9 (Table 1).

The effects of turbulence are pronounced in the cases of $\gamma = 10^{-1}$ (Fig. 5c) and $\gamma = 1$ (Fig. 5d). The random walk and eccentricity excitation induced by the turbulence tend to inhibit isolation of the planets. In Fig. 5c (RUN2_{1a}), the duration of orbit crossing is elongated, while 8 planets still survive. (The same number of planets survive also in RUN2_{1b} and RUN2_{1c}.) According to the eccentricity excitation effect, the eccentricities of final planets are slightly larger than in the previous two cases, however, they are still smaller than the present free eccentricities of Earth and Venus, because the damping that increases with planet mass eventually overwhelms the turbulent excitation that is independent of the planet mass. In Fig. 5d (RUN2_{0a} with $\gamma = 1$), the large random walk enhances the number of collision events (10 events), so that the number of surviving planets drastically decreases to 4. In RUN2_{0b} and RUN2_{0c}, the number of surviving planets is also 4 or 5.

In Fig. 5d ($\gamma = 1$), secular inward migration is found, although type-I migration is not included. This migration is induced by the damping of eccentricities that are continuously excited by the random torques, since orbital angular momentum, $\sqrt{G M_\odot a(1-e^2)}$, is almost conserved during the eccentricities damping. In the run with extremely large γ (=10), the turbulent excitation is so strong that all the planets are removed from terrestrial planet region by the inward migration.

3.2.2. Case with $f_g = 10^{-4}$

The evolution in severely depleted disks with $f_g = 10^{-4}$, RUN$4_{\infty a}$, RUN4_{3a}, RUN4_{1a}, and RUN4_{0a} is shown in Figs. 6a,

Table 1
Initial parameters and final results for each run

RUN	f_g	γ	Type-I	$M_1 (M_\oplus)$	e_1	Collision events	Number of final planets
RUN2$_{\infty a}$	10^{-2}	0	No	0.6	0.0001	7	8
RUN2$_{\infty b}$	10^{-2}	0	No	0.8	0.0004	7	8
RUN2$_{\infty c}$	10^{-2}	0	No	0.8	0.0001	6	9
RUN2$_{3a}$	10^{-2}	10^{-3}	No	0.6	0.002	7	8
RUN2$_{3b}$	10^{-2}	10^{-3}	No	0.8	0.003	6	9
RUN2$_{3c}$	10^{-2}	10^{-3}	No	0.8	0.0002	6	9
RUN2$_{1a}$	10^{-2}	10^{-1}	No	0.8	0.003	7	8
RUN2$_{1b}$	10^{-2}	10^{-1}	No	0.8	0.003	7	8
RUN2$_{1c}$	10^{-2}	10^{-1}	No	0.8	0.003	7	8
RUN2$_{0a}$	10^{-2}	1	No	1.2	0.02	10	5
RUN2$_{0b}$	10^{-2}	1	No	1.0	0.02	11	4
RUN2$_{0c}$	10^{-2}	1	No	1.0	0.02	10	5
RUN4$_{\infty a}$	10^{-4}	0	No	1.4	0.01	9	6
RUN4$_{\infty b}$	10^{-4}	0	No	1.2	0.001	7	8
RUN4$_{\infty c}$	10^{-4}	0	No	1.2	0.003	10	5
RUN4$_{3a}$	10^{-4}	10^{-3}	No	1.6	0.01	10	5
RUN4$_{3b}$	10^{-4}	10^{-3}	No	1.2	0.01	11	4
RUN4$_{3c}$	10^{-4}	10^{-3}	No	1.2	0.02	8	7
RUN4$_{3d}$	10^{-4}	10^{-3}	No	1.0	0.02	8	7
RUN4$_{1a}$	10^{-4}	10^{-1}	No	1.2	0.008	9	6
RUN4$_{1b}$	10^{-4}	10^{-1}	No	1.8	0.004	10	5
RUN4$_{1c}$	10^{-4}	10^{-1}	No	1.0	0.02	9	6
RUN4$_{0a}$	10^{-4}	1	No	1.6	0.01	11	4
RUN4$_{0b}$	10^{-4}	1	No	1.6	0.008	10	5
RUN4$_{0c}$	10^{-4}	1	No	1.2	0.01	10	5
RUN2$_{\infty a\mathrm{I}}$	10^{-2}	0	Yes	0.4	0.005	7	3 ($t = 10^7$ years)
RUN2$_{3a\mathrm{I}}$	10^{-2}	10^{-3}	Yes	0.2	0.0001	9	1 ($t = 10^7$ years)
RUN2$_{1a\mathrm{I}}$	10^{-2}	10^{-1}	Yes	0.4	0.01	6	5 ($t = 10^7$ years)
RUN2$_{0a\mathrm{I}}$	10^{-2}	1	Yes	0.2	0.02	10	1 ($t = 10^7$ years)

Note. M_1 is the mass of the largest planet in final state. e_1 is the time averaged eccentricity of the largest planet, taken after its isolation takes place.

6b, 6c, and 6d, respectively. $f_g = 10^{-4}$ corresponds to $\tau_{\mathrm{damp}} \simeq 1.2 \times 10^7$ years for $M = 0.2M_\oplus$. RUN4$_{\infty a}$ shows the result without the effect of turbulence. The weak damping due to the small surface density of a gas disk elongates the period during which the eccentricities are high enough to allow orbital crossing ($\sim 1 \times 10^7$ years). As a result, a larger planet ($M = 1.4M_\oplus$) than in RUN2$_{\infty a}$ is formed. Since e is damped down to ~ 0.01, this planet is very similar to Earth. However, the number of surviving planets is 6 (Fig. 6a), which is larger than that in the present Solar System, as is the case shown by Kominami and Ida (2002). The mean number of surviving planets of RUN4$_{\infty a}$, RUN4$_{\infty b}$, and RUN4$_{\infty c}$ is 6.3.

In the turbulence cases, the mean number of surviving planets is 5.8 ($\gamma = 10^{-3}$), 5.7 ($\gamma = 10^{-1}$), and 4.7 ($\gamma = 1$). As the turbulence becomes stronger, the number of final planets decreases. In RUN4$_{1a}$ with $\gamma = 10^{-1}$, global orbital crossing lasts on more than 10^7 years (Fig. 6c), while RUN4$_{3a}$ does not show such clear elongation of orbital crossing (Fig. 6b). The turbulent excitation for eccentricities is still weaker than the tidal damping for Earth-mass planets as long as $\gamma \leqslant 1$, so that their final eccentricities are still $\lesssim 0.01$. (In the run with extremely large γ (=10), we found that the eccentricities are not sufficiently damped.) In general, probability for final planets to be similar to present terrestrial planets in our Solar System is larger for $f_g = 10^{-4}$ than for $f_g = 10^{-2}$.

The accretion timescales in weak turbulence cases are a few times 10^6 years after orbit crossing starts. Those in strong turbulence cases are $\sim 10^7$ years. Iwasaki et al. (2002) and Kominami and Ida (2002) suggested that orbit crossing does not start until f_g decays down to $\sim 10^{-3}$. If the effect of turbulence is taken into account, orbit crossing may start at the stage of larger f_g. If the condition of $f_g \lesssim 10^{-3}$ is applied and exponential decay from initial $f_g \sim 1$ with decay timescale τ_{dep} is assumed, the orbit crossing starts at $\sim 7\tau_{\mathrm{dep}} \sim 10^7$–$10^8$ years. Thus, the total accretion timescales in the present model are not in contradiction to the Earth formation age inferred from Hf–W chronology $\sim 4 \times 10^7$ years (Yin et al., 2002; Yin and Ozima, 2003; Kleine et al., 2002, 2004).

If disk depletion is only due to viscous diffusion, it may be possible that such small-mass remnant disks remain for 10^7–10^8 years. However, if disk dispersal due to stellar EUV is efficient, it would be difficult to preserve such small-mass remnant disks. Spitzer survey found that 25% of B–A members and 10% of F–K members in Pleiades cluster show IR excess (Nadya et al., 2006). The excess might imply the existence of small-mass remnant gas disks, but it might also be due to secondary dust generation in gas free environments. Observation of gas components for clusters at 10^7–10^8 years is needed to examine the role of the tidal damping due to remnant disks on final orbital configuration of terrestrial planets.

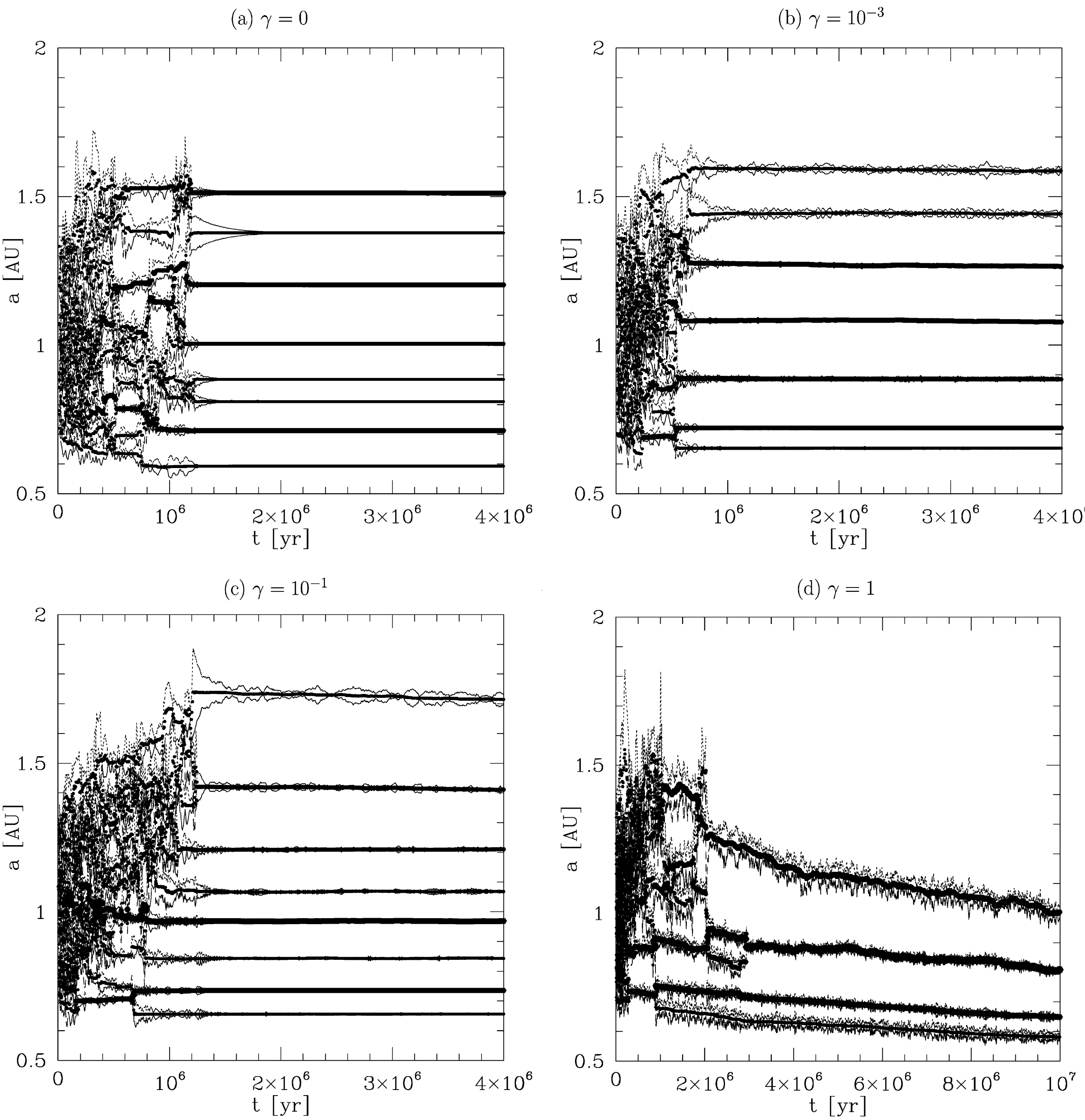

Fig. 5. The results of N-body simulations with $f_g = 10^{-2}$. (a) $\gamma = 0$ [RUN$2_{\infty a}$], (b) $\gamma = 10^{-3}$ [RUN2_{3a}], (c) $\gamma = 10^{-1}$ [RUN2_{1a}], and (d) $\gamma = 1$ [RUN2_{0a}]. The thick solid lines represent semimajor axes a. The thin dashed lines represent pericenters $a(1-e)$ and apocenters $a(1+e)$. Thicker solid lines represent more massive planets.

3.2.3. Eccentricities and feeding zones

Once orbit crossing starts, the velocity dispersion is pumped up to surface escape velocity $v_{\rm esc}$ of planets by close encounters. Corresponding eccentricity is given by

$$e \sim \frac{v_{\rm esc}}{v_{\rm K}} = 0.34\left(\frac{\rho_P}{3\ {\rm g\,cm^{-3}}}\right)^{1/6}\left(\frac{M}{M_\oplus}\right)^{1/3}\left(\frac{a}{1\ {\rm AU}}\right)^{1/2}. \quad (37)$$

Fig. 7 shows eccentricity evolution of all bodies in RUN$2_{\infty a}$ (non-turbulent case) and RUN2_{0a} (strongly turbulent case with $\gamma = 1$). During orbit crossing ($t \lesssim 1\times10^6$ years), the mean eccentricities are almost same in the two cases. Since eccentricity excitation due to random torques evaluated by Eq. (34) is significantly smaller than Eq. (37), the eccentricities during orbit crossing are mostly determined by mutual planetary perturbations.

In RUN$2_{\infty a}$, global orbit crossing ceases at $t \gtrsim 1\times10^6$ years and then the eccentricities are secularly decreased by the damping due to $\boldsymbol{F}_{\rm damp}$. However, in RUN$2_{0a}$, close encounters still occasionally occur at $t \gtrsim 1\times10^6$ years, so that the eccentricity damping is slower. Even with relatively strong turbulence of $\gamma = 1$ of this run, the tidal damping of eccentricities overcomes the turbulent excitation for Earth-mass planets. (But, this is not the case for $\gamma = 10$.)

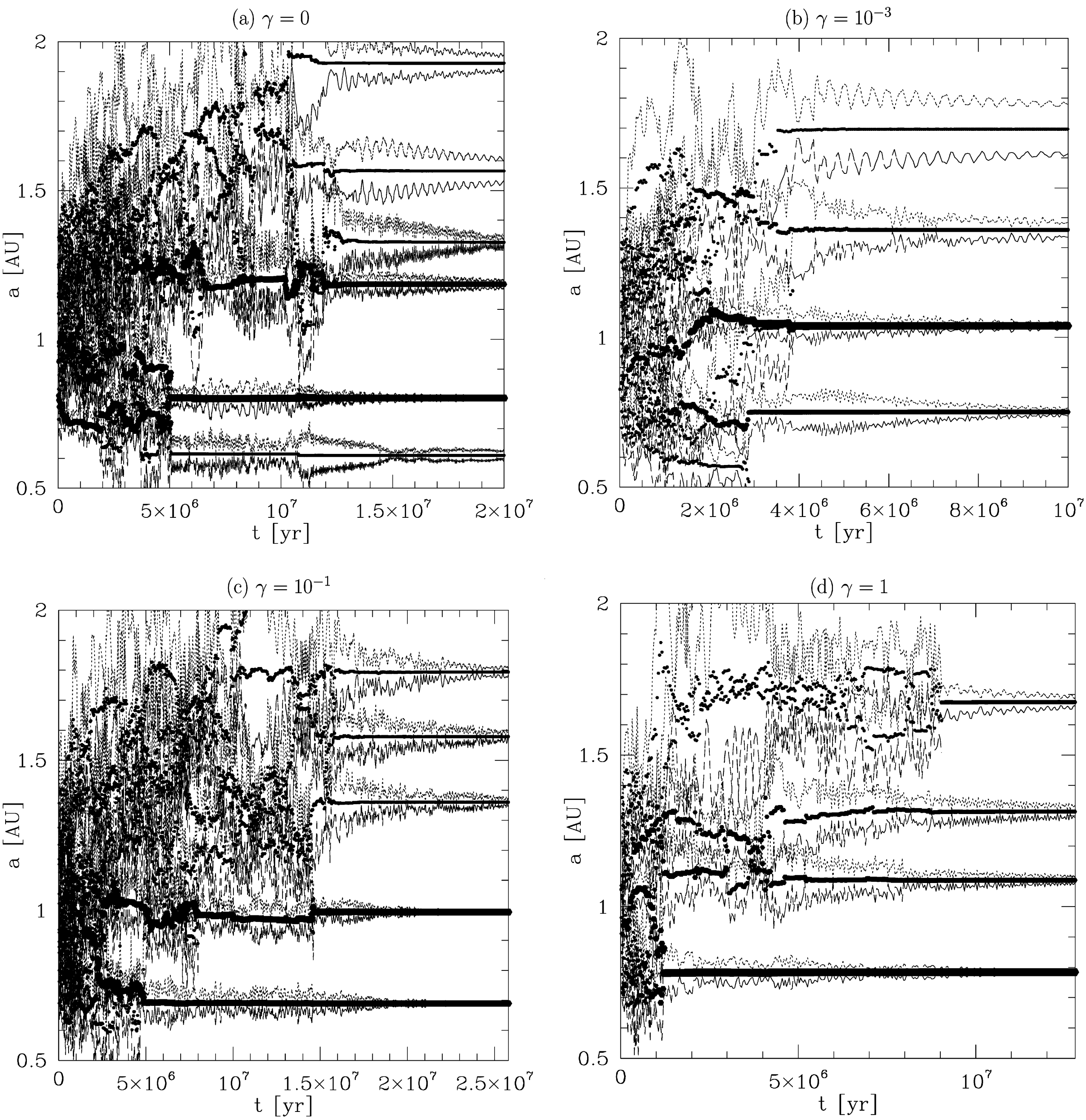

Fig. 6. The results of N-body simulations with $f_g = 10^{-4}$. (a) $\gamma = 0$ [RUN4$_{\infty a}$], (b) $\gamma = 10^{-3}$ [RUN4$_{3a}$], (c) $\gamma = 10^{-1}$ [RUN4$_{1a}$], and (d) $\gamma = 1$ [RUN4$_{0a}$]. The meaning of lines is the same as in Fig. 5.

For $\gamma = 1$ and $f_g = 10^{-2}$, diffusion length due to random torques is evaluated by Eq. (33) as $\Delta a \sim 10^{-2}(t/10^6\ \text{year})^{1/2}$ AU, which is much smaller than orbital separation among the protoplanets. However, as suggested before, planetary perturbations may inhibit cancellation of the torques and induce much larger Δa (and e). Furthermore, even if the turbulence itself does not directly expand the feeding zones of the planets, scattering by close encounters among protoplanets that are induced by the random torques allows the feeding zones to effectively expand. In the N-body simulations, the two effects are indistinguishable.

3.2.4. Effects of type-I migration

Here, the results with type-I migration (calculations with $\boldsymbol{F}_{\text{mig}}$) are shown, although it is not clear that type-I migration actually operates in turbulent disks (Nelson, 2005). In RUN2$_{\infty a\text{I}}$, $f_g = 10^{-2}$ and the turbulence is not included ($\gamma = 0$). More systematic investigations in the non-turbulence cases were done by McNeil et al. (2005) and Daisaka et al. (2006). Although McNeil et al. (2005) and Daisaka et al. (2006) included the effects of small planetesimals as well, RUN2$_{\infty a\text{I}}$ shows similar properties to their calculations (Fig. 8a): planets in inner regions tend to fall onto the host stars while those in outer re-

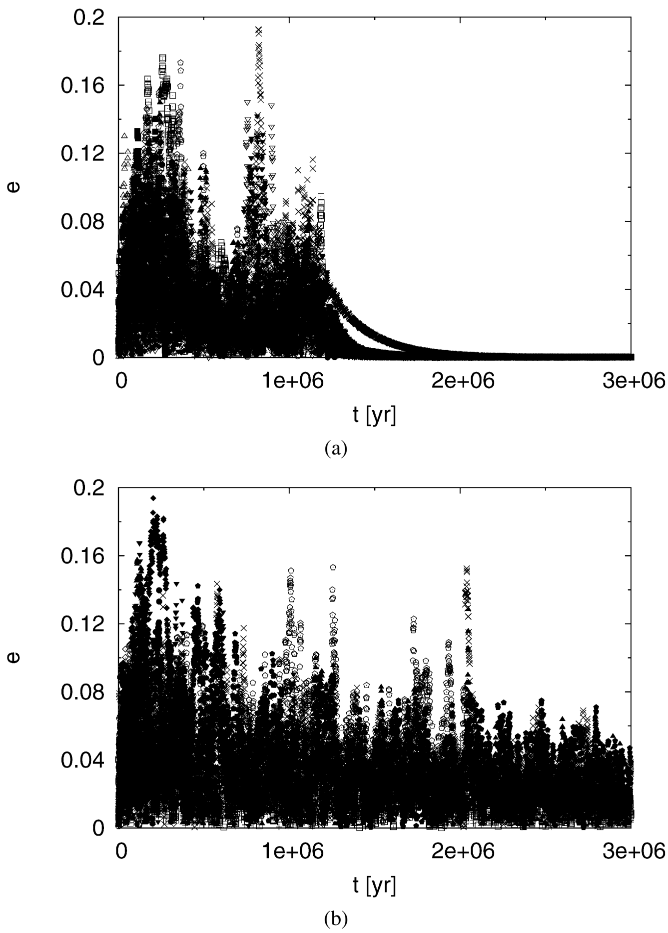

Fig. 7. The eccentricity evolution of all bodies: (a) $\gamma = 0$ [RUN2$_{\infty a}$] and (b) $\gamma = 1$ [RUN2$_{0a}$].

gions could survive. Since collision events are limited by the loss of inner planets, the mass of the largest surviving planets is $0.4M_\oplus$. (Inclusion of protoplanets in more outer region might increase the mass of final planets.)

Figs. 8b and 8c show RUN2$_{1aI}$ of $\gamma = 10^{-1}$ and RUN2$_{0aI}$ of $\gamma = 1$. Even with relatively strong turbulence, the tendency to migrate inward does not change, compared with the non-turbulent case in Fig. 8a. Equation (36) shows that type-I migration is dominant over the random walk after $t \sim 3 \times 10^5 \gamma^2 (M/0.2M_\oplus)^{-2}$ years, so that the random walk cannot halt the inward migration on timescales $\sim 10^6$ years. The inward migration is rather accelerated by the damping of eccentricities that are continuously excited by the random torques (Section 3.2.1).

For larger f_g, since the random torques are stronger, the accelerated migration is more pronounced. Thus, our results suggest that random migration superposed to type-I migration would not be able to solve the problem that planets tend to be lost from the terrestrial planet region. The problem can be solved only if the turbulent fluctuations somehow inhibit the underlying type-I migration, as found by Nelson (2005), or if planets at ~ 1 AU are formed by surviving protoplanets originally at >1 AU.

4. Conclusions

We have investigated the final accretion stage of terrestrial planets from Mars-mass protoplanets in turbulent disks, through N-body simulation. Gravitational interactions with gas disks exert the following three effects on the protoplanet orbits:

(1) damping of eccentricities e and inclinations i,
(2) type-I migration (secular decrease of semimajor axis a),
(3) random-walks of a and stochastic excitation of e.

The effect (3) has not been included in N-body simulations of planet accretion in the previous works. We adopt the same simulation setting of Kominami and Ida (2002) that included only the effect (1): initially 15 protoplanets of $0.2M_\oplus$ are set with orbital separations of several Hill radii in terrestrial planet regions, corresponding to MMSN. In our N-body simulations, the effects (1) and (3) were included. The effect (2) was examined in Section 3.2.4. We incorporated random torques exerted by disk turbulence due to MRI as forces directly acting on protoplanets in the equations of motion for orbital integration. We adopted the semi-analytical formula for the random torques developed by Laughlin et al. (2004) with slight modifications. Compared with the results of Kominami and Ida (2002), we investigated the effects of disk turbulence on planet accretion.

The past N-body simulations neglecting the gas disk showed that the coagulation between protoplanets result in planets of about Earth-mass but with the eccentricities higher than the present terrestrial planets in our Solar System. If the effect (1) is included, when $\Sigma_g \sim 10^{-4}$–$10^{-3} \Sigma_{g,\mathrm{MMSN}}$, the damping allows initiation of orbit crossing to form an Earth-mass planet(s), while it damps the eccentricities sufficiently after planets are isolated. However, $\gtrsim 6$ planets tend to remain, because of isolation due to the damping (Kominami and Ida, 2002). [Note that in the case of damping by dynamical friction from remnant planetesimals the number of planets is reduced (O'Brien et al., 2006).] We found that the newly incorporated effect (3) tends to inhibit isolation of planets, resulting in more coagulations of planets, while the eccentricity damping is still effective. As a result, 4–5 planets with small eccentricities are formed in relatively wide parameter range: gas surface density $\Sigma_g \sim 10^{-4}$–$10^{-2} \Sigma_{g,\mathrm{MMSN}}$, and MRI turbulence strength $\gamma \sim 10^{-1}$–1 (slightly smaller γ if $m = 1$ modes of density fluctuation are included).

Laughlin et al.'s (2004) prescription for the random torques that we adopted has highly symmetric properties and the exerted torques almost completely cancel out in time averaging. As a result, the diffusion length and eccentricity excitation obtained by one planet calculations are generally too small to play a direct role in expanding feeding zones of protoplanets in late phase in which disk gas is significantly depleted (Eqs. (33) and (34)). However, planetary perturbations may break the symmetry. Furthermore, in more realistic turbulence, the torques may include $m = 1$ modes and be less symmetric. These effects inhibit the torque cancellation to induce much larger Δa and e.

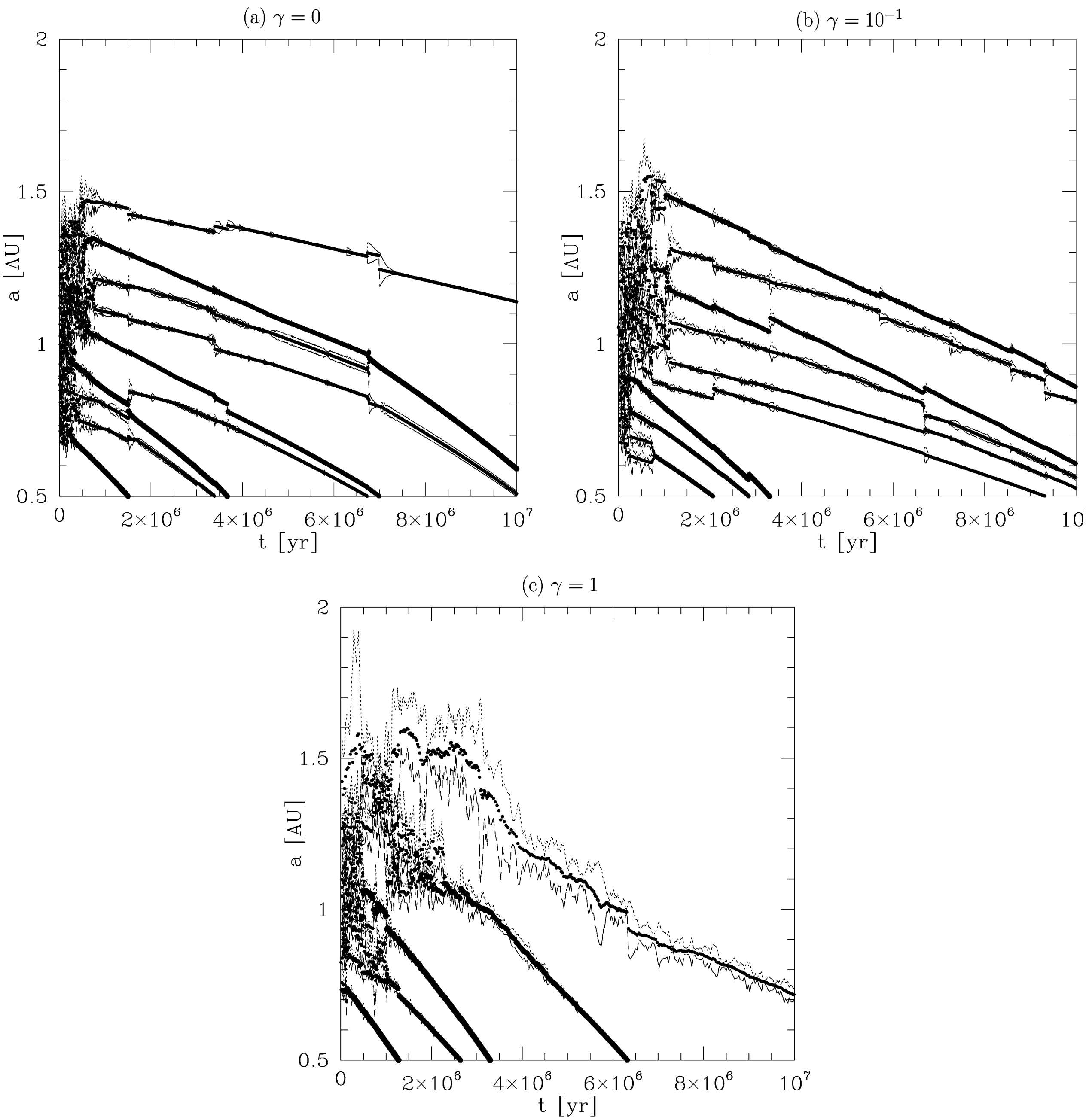

Fig. 8. The results of N-body simulations with $f_g = 10^{-2}$, including type-I migration. (a) $\gamma = 0$ [RUN2$_{\infty a\mathrm{I}}$], (b) $\gamma = 10^{-1}$ [RUN2$_{1a\mathrm{I}}$], and (c) $\gamma = 1$ [RUN2$_{0a\mathrm{I}}$]. The meaning of lines, see caption of Fig. 5.

Furthermore, even if the enhanced effects are still too small to directly expand the feeding zones, such small effects can be enough to break the isolation of the protoplanets, thus allowing them to have distant encounters with each other. The encounters in turn induce larger random oscillations of the semimajor axes, effectively enhancing the feeding zone of each planet. We also found through calculations with all the effects (1), (2), and (3) that the random walks do not decelerate (rather accelerate) the type-I migration, although it is not clear that type-I migration actually operates in turbulent disks.

Although the prescription for the random torques would include large uncertainty, we have demonstrated that the random torques tend to decrease number of final planets while they keep formation of Earth-mass planets with small eccentricities, which is more consistent with the present Solar System. Since the random torques are independent of mass of bodies, small planetesimals also suffer the random torques. N-body simulations starting from smaller planetesimals in turbulent disks will be presented in a separate paper.

Acknowledgments

We thank Fred Adams and Greg Laughlin for detailed and useful comments on the random torque functions. We also thank an anonymous referee for helpful comments.

References

Agnor, C.B., Canup, R.M., 1999. On the character and consequences of large impacts in the late stage of terrestrial planet formation. Icarus 142, 219–237.

Agnor, C.B., Ward, W.R., 2002. Damping of terrestrial planet eccentricities by density wave interactions with a remnant gas disk. Astrophys. J. 567, 579–586.

Artymowicz, P., 1993. Disk–satellite interaction via density waves and the eccentricity evolution of bodies embedded in disks. Astrophys. J. 419, 166–180.

Balbus, S.A., Hawley, J.F., 1991. A powerful local shear instability in weakly magnetized disks. I. Linear analysis. II. Nonlinear evolution. Astrophys. J. 376, 214–233.

Chambers, J.E., 2001. Making more terrestrial planets. Icarus 152, 205–224.

Chambers, J.E., Wetherill, G.W., 1998. Making the terrestrial planets: N-body integrations of planetary embryos in three dimensions. Icarus 136, 304–327.

Chambers, J.E., Wetherill, G.W., Boss, A.P., 1996. The stability of multi-planet systems. Icarus 119, 261–268.

Daisaka, K.J., Tanaka, H., Ida, S., 2006. Orbital evolution and accretion of protoplanets tidally interacting with a gas disk. II. Solid surface density evolution with type-I migration. Icarus 185, 492–507.

Gammie, C.F., 1996. Layered accretion in T Tauri disks. Astrophys. J. 457, 355–362.

Hartmann, L., Calvet, N., Gullbring, E., D'Alessio, P., 1998. Accretion and the evolution of T Tauri disks. Astrophys. J. 495, 385–400.

Hayashi, C., 1981. Structure of the solar nebula, growth and decay of magnetic fields and effects of magnetic and turbulent viscosities on the nebula. Prog. Theor. Phys. Suppl. 70, 35–53.

Ida, S., Lin, D.N.C., 2004. Toward a deterministic model of planetary formation. I. A desert in the mass and semimajor axis distributions of extrasolar planets. Astrophys. J. 604, 388–413.

Inaba, S., Wetherill, G.W., Ikoma, M., 2003. Formation of gas giant planets: Core accretion models with fragmentation and planetary envelope. Icarus 166, 46–62.

Inutsuka, S., Sano, T., 2005. Self-sustained ionization and vanishing dead zones in protoplanetary disks. Astrophys. J. 628, 155–158.

Iwasaki, K., Emori, H., Nakazawa, K., Tanaka, H., 2002. Orbital stability of a protoplanet system under a drag force proportional to the random velocity. Publ. Astron. Soc. Jpn. 54, 471–479.

Johnson, E.T., Goodman, J., Menou, K., 2006. Diffusive migration of low-mass protoplanets in turbulent disks. Astrophys. J. 647, 1413–1425.

Kleine, T., Münker, C., Mezger, K., Palme, H., 2002. Rapid accretion and early core formation on asteroids and the terrestrial planets from Hf–W chronometry. Nature 418, 952–955.

Kleine, T., Mezger, K., Palme, H., Münker, C., 2004. The W isotope evolution of the bulk silicate Earth: Constraints on the timing and mechanisms of core formation and accretion. Earth Planet. Sci. Lett. 228, 109–123.

Kokubo, E., Ida, S., 1998. Oligarchic growth of protoplanets. Icarus 131, 171–178.

Kokubo, E., Ida, S., 2000. Formation of protoplanets from planetesimals in the solar nebula. Icarus 143, 15–27.

Kominami, J., Ida, S., 2002. The effect of tidal interaction with a gas disk on formation of terrestrial planets. Icarus 157, 43–56.

Kominami, J., Ida, S., 2004. Formation of terrestrial planets in a dissipating gas disk with Jupiter and Saturn. Icarus 167, 231–243.

Kominami, J., Tanaka, H., Ida, S., 2005. Orbital evolution and accretion of protoplanets tidally interacting with a gas disk. I. Effects of interaction with planetesimals and other protoplanets. Icarus 178, 540–552.

Laughlin, G., Steinacker, A., Adams, F.C., 2004. Type I planetary migration with MHD turbulence. Astrophys. J. 608, 489–496.

Levison, H.F., Agnor, C., 2003. The role of giant planets in terrestrial planet formation. Astron. J. 125, 2692–2713.

Lissauer, J.J., 1987. Timescales for planetary accretion and the structure of the protoplanetary disk. Icarus 69, 249–265.

McNeil, D., Duncan, M., Levison, H.F., 2005. Effects of type I migration on terrestrial planet formation. Astron. J. 130, 2884–2899.

Nadya, G., Rieke, G.H., Muzerolle, J., Stauffer, J.R., Siegler, N., Young, E.T., Stansberry, J.H., 2006. Spitzer 24 μ survey of debris disks in the Pleiades. Astrophys. J. 649, 1028–1042.

Nagasawa, M., Lin, D.N.C., Thommes, E., 2005. Dynamical shake-up of planetary systems. I. Embryo trapping and induced collisions by the sweeping secular resonance and embryo–disk tidal interaction. Astrophys. J. 635, 578–598.

Nelson, R.P., 2005. On the orbital evolution of low mass protoplanets in turbulent, magnetized disks. Astron. Astrophys. 443, 1067–1085.

Nelson, R.P., Papaloizou, J.C.B., 2004. The interaction of giant planets with a disc with MHD turbulence. IV. Migration rates of embedded protoplanets. Mon. Not. R. Astron. Soc. 350, 849–864.

O'Brien, D.P., Morbidelli, A., Levison, H.F., 2006. Terrestrial planet formation with strong dynamical friction. Icarus 184, 39–58.

Papaloizou, J.C.B., Larwood, J.D., 2000. On the orbital evolution and growth of protoplanets embedded in a gaseous disc. Mon. Not. R. Astron. Soc. 530, 823–833.

Raymond, S.N., Barnes, R., Kaib, N.A., 2006. Predicting planets in known extrasolar planetary systems. III. Forming terrestrial planets. Astrophys. J. 644, 1223–1231.

Rice, W.K.M., Armitage, P.J., 2003. On the formation timescale and core masses of gas giant planets. Astrophys. J. 598, L55–L58.

Sano, T., Miyama, S.M., Umebayashi, T., Nakano, T., 2000. Magnetorotational instability in protoplanetary disks. II. Ionization state and unstable regions. Astrophys. J. 543, 486–501.

Tanaka, H., Ward, W.R., 2002. Three-dimensional interaction between a planet and an isothermal gaseous disk. I. Corotation and Lindblad torques and planet migration. Astrophys. J. 565, 1257–1274.

Tanaka, H., Ward, W.R., 2004. Three-dimensional interaction between a planet and an isothermal gaseous disk. II. Eccentricity waves and bending waves. Astrophys. J. 602, 388–395.

Ward, W.R., 1986. Density waves in the solar nebula—Differential Lindblad torque. Icarus 67, 164–180.

Ward, W.R., 1993. Density waves in the solar nebula—Planetesimal velocities. Icarus 106, 274–287.

Ward, W.R., 1997. Survival of planetary systems. Astrophys. J. 482, L211–L214.

Yin, Q., Ozima, M., 2003. Hf–W and I–Xe ages and the planetary formation timescale. Geochim. Cosmochim. Acta Suppl. 67, 564.

Yin, Q., Jacobsen, S.B., Yamashita, K., Blichert-Toft, J., Télouk, P., Albarède, F., 2002. A short timescale for terrestrial planet formation from Hf–W chronometry of meteorites. Nature 418, 949–952.

Yoshinaga, K., Kokubo, E., Makino, J., 1999. The stability of protoplanet systems. Icarus 139, 328–335.